Arabian Journal of Geosciences (2020) 13: 1030
https://doi.org/10.1007/s12517-020-06000-7

S. I. GSF 2018

Seismic monitoring and high-frequency noise using arrays in the Arabian Peninsula

Moira L. Pyle[1] · Rengin Gök[1] · Abdullah Al-Amri[2] · Issa El-Hussain[3] · Yasir Al-Rawahi[3]

Received: 27 April 2020 / Accepted: 10 September 2020 / Published online: 26 September 2020

Abstract

Seismic arrays provide useful tools for regional seismic monitoring. Two small-aperture, regionally-oriented arrays, QWAR and HQAR, were deployed in Saudi Arabia and Oman in 2012 and 2016. We utilize a time-domain beampacking method, similar to frequency-wavenumber analysis, to examine the performance of the arrays in terms of slowness and azimuthal bias and event detection capabilities. Additionally, we investigate persistent ambient noise sources recorded by the arrays. We find that the arrays provide slowness vectors with biases comparable with similar-sized arrays of the International Monitoring System in other locations around the world. At QWAR, regional events of magnitude 3.0 and above are detected a majority of the time, and as magnitudes increase to 4.0 and above, the detection rate is greater than 82%. Strong noise generation, primarily with slownesses characteristic of Lg waves, is found in the directions of the northern Arabian/Persian Gulf and southern Red Sea and may be a factor in event detection capabilities.

Keywords Array analysis · Seismic noise · Beamforming · Event detection

Introduction

The Middle East is a complicated tectonic region with large amounts of active seismicity. Seismic monitoring and improved methods for detecting and locating earthquakes are key to a better understanding of local seismic hazard. While many seismic networks are already in place in the region and its surrounding, the addition of small-aperture seismic arrays can provide additional tools for the monitoring process. Arrays provide information on the direction of incoming energy in the form of an apparent velocity and backazimuth direction that allows for distinctions between different seismic phases with different ray parameters as well as back-projection to source regions. Additionally, arrays can provide similar information about ambient seismic noise, which can aid in a better understanding of detection limitations.

As part of capacity building and joint research efforts of the Seismic Cooperation Program at Lawrence Livermore National Laboratory, two arrays were collaboratively installed in Saudi Arabia in 2012 and Oman in 2015 (Fig. 1). The arrays, located on the relatively stable Arabian Peninsula, are surrounded by divergent, transform, and convergent plate boundaries, placing them in a prime location to aid in regional event detection. The movement of the Arabian Plate away from the African Plate and in collision with the Eurasian Plate forms boundaries at the Bitlis suture zone to the north, the Zagros suture zone to the northeast, and the Makran subduction zone to the east. Beyond the suture zones to the north and east, the Turkish and Iranian Plateau is a young and active collision zone (Dewey et al. 1986). To the south and southeast, the Gulf of Aden forms a divergent boundary, and the Arabian Plate is separated from the Indian Plate by the Owen-Murray Fracture zone transform boundary to the southeast (Al-Hashmi et al. 2011). The Dead Sea fault System and the east Anatolian fault are situated to the west and northwest (Bao et al. 2011). The complex tectonic terrains that lead to these many boundaries result in a great deal of active seismicity as well as large variations in crustal properties that may affect the detection and location of that seismicity.

Prepared for submission to Arabian Journal of Geosciences, LLNL-JRNL-808484

This article is part of the Topical Collection on *Seismic and Earthquake Engineering Studies in the Arabian Plate and the Surrounding Region*

✉ Moira L. Pyle
pyle4@llnl.gov

[1] Lawrence Livermore National Laboratory, Livermore, CA 94550, USA

[2] King Saud University, Riyadh, Saudi Arabia

[3] Sultan Qaboos University, Muscat, Oman

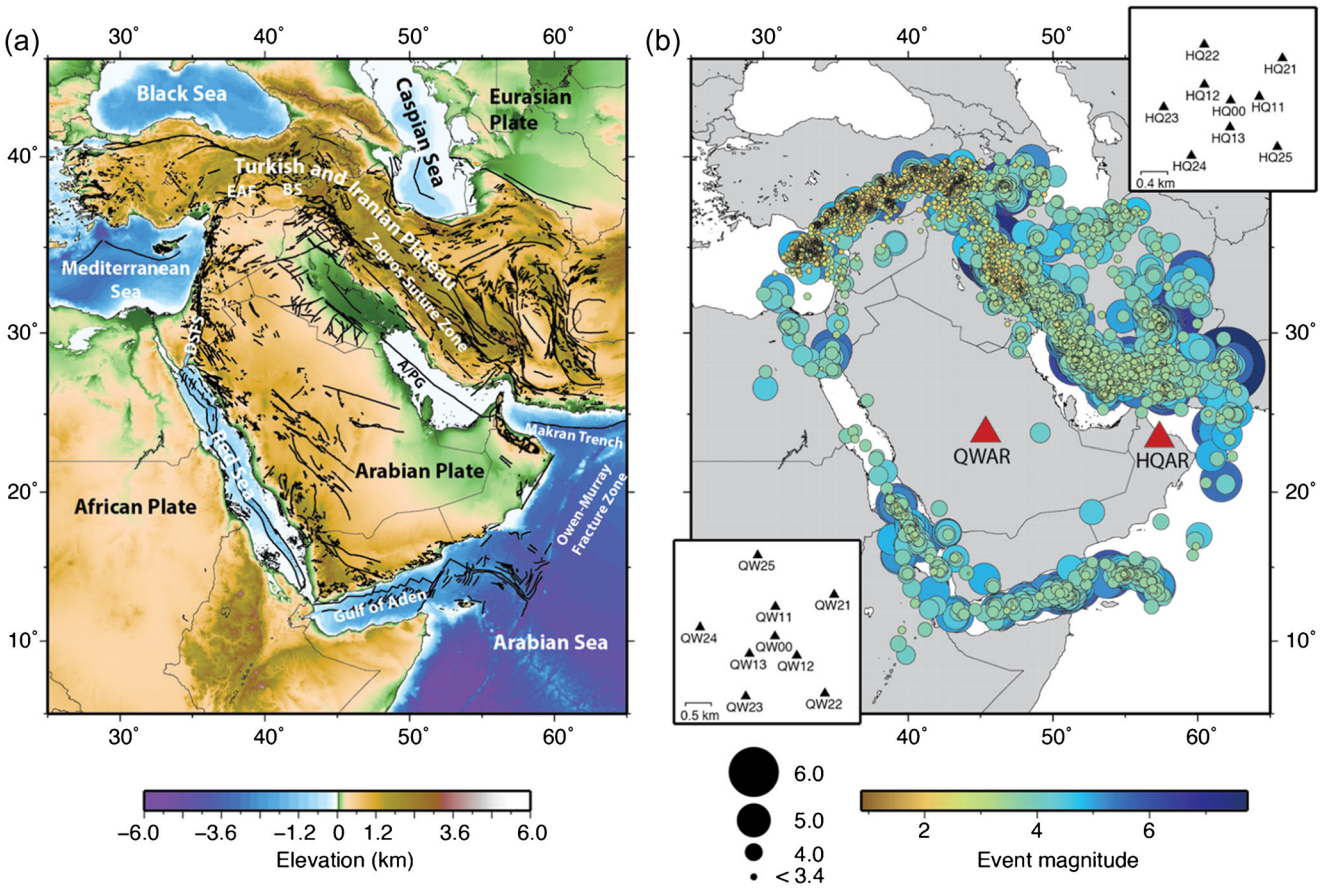

Fig. 1 **a** Regional topographic map. A/PG, Arabian/Persian Gulf; BS, Bitlis suture; DSFS, Dead Sea fault system; EAF, East Anatolian fault. **b** Map of station and event locations. Red triangles indicate location of the QWAR and HQAR arrays and circles (color coded and scaled by event magnitude) indicate location of earthquakes used in the study. Top and bottom insets show layout of individual elements for the two arrays

The installed arrays each consist of 9 elements positioned in concentric rings in the style of many of the smaller International Monitoring System (IMS) arrays (Fig. 1b). The aperture of each array is approximately 3.5 km with a minimum element spacing of ~ 0.5 km. All elements are equipped with 3-component, short period SS-1 sensors and Q330 Kinemetrics digitizers and record at 100 sps. The QWAR array is located on the Arabian Shield just west of the Arabian platform. The HQAR array is located on the Semail ophiolite, adjacent to the foothills of the Al Hajar Al Gharbi mountains. Unfortunately, telecommunication problems limited the collection of data from several of the elements in the HQAR array, diminishing the resolution capabilities of the array. Because of this, we focus our analysis on the QWAR array, investigating the performance of the array, detection capabilities, and the influence of nearby ambient seismic noise.

Data and methods

We assemble a data set of earthquakes spanning the time from April 2012 through January 2018 that are listed in the catalogs of the International Data Centre (IDC) in Austria, the International Seismological Centre (ISC) in the United Kingdom, the Kandilli Observatory and Earthquake Research Institute (KOERI) in Turkey, and the National Earthquake Information Center (NEIC) in the United States. Events are limited to within 16° of the QWAR array to assess the regional detection capabilities and array analysis performance. We obtain a total of 7344 events (Fig. 1b) ranging in magnitude from 0.6 to 7.3, with 80% of the magnitudes falling between 1.0 and 4.0. Magnitude types depend upon what is reported by the various catalogs, but most events have either a local magnitude (M_L) or a surface wave magnitude (M_S). The events have wide azimuthal coverage, but locations are heavily weighted from approximately 300° to about 90° in backazimuth from the array, in the directions of the Bitlis and Zagros suture zones.

In performing array analysis, it is important to consider the array size, which determines the frequencies for which the array is most useful. The small aperture of QWAR and HQAR makes them primarily suitable for high-frequency regional signals. We select a frequency band of 1–4 Hz as our preferred frequency band for analysis based on the array response function. Below 1 Hz, the main lobe of the array response becomes very large, making it difficult to distinguish

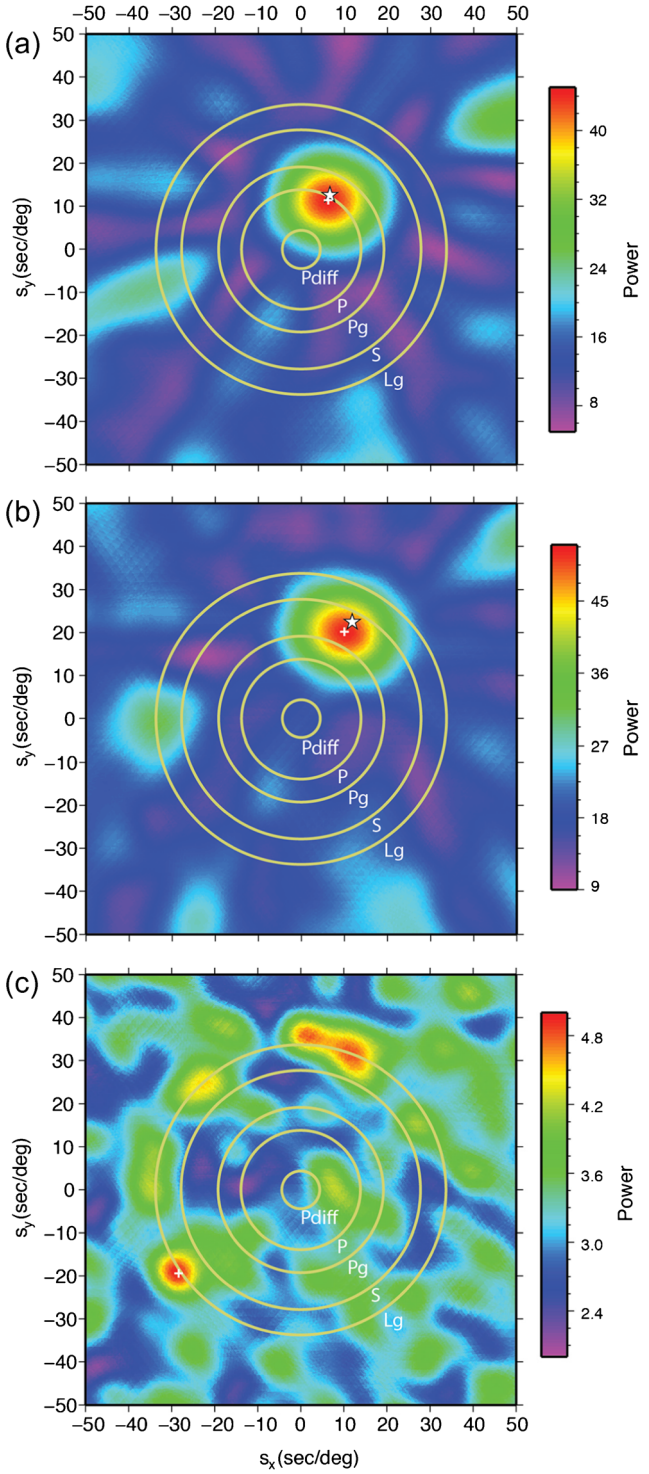

Fig. 2 Examples of the power vs. slowness grids obtained from the beampacking analysis for a magnitude 3.4 event located 932 km to the northeast of QWAR for the **a** P window, **b** S window, and **c** noise window. In all cases, the white cross indicates the location of the optimal slowness vector, and for the P and S windows, the white star indicates the theoretical slowness vector. Concentric circles show expected slownesses for phases Pdiff, P, Pg, S, and Lg for reference

between slownesses of different arrivals, and above 4 Hz, the side lobes become strong and numerous which can lead to

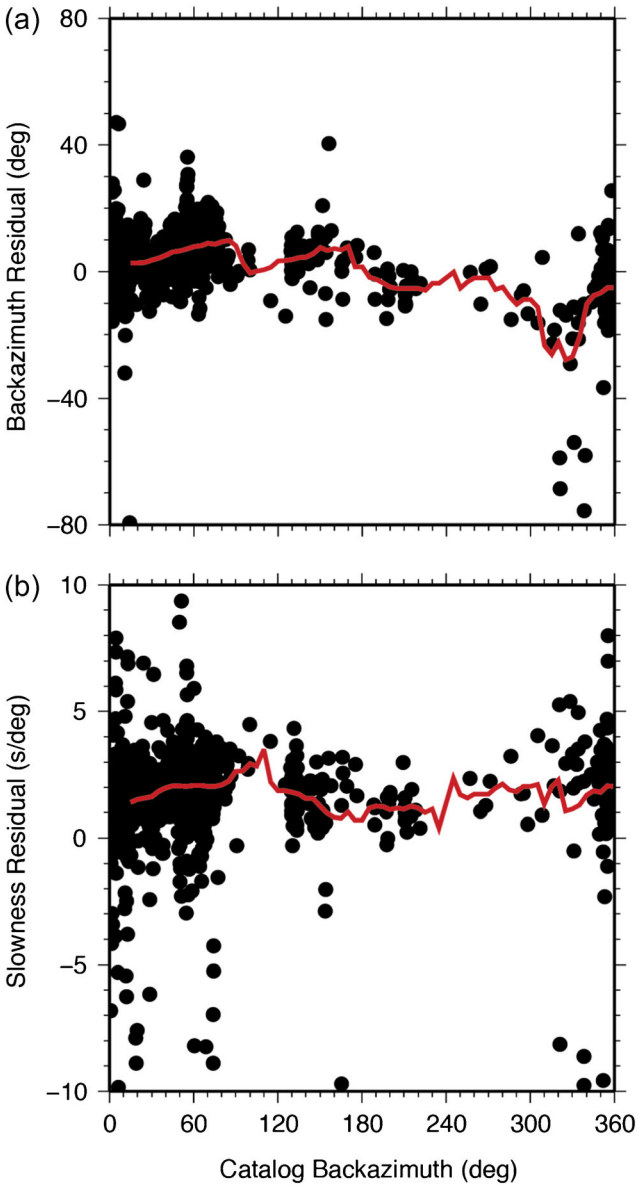

Fig. 3 Residuals for events with a beam signal-to-noise ratio of 2.0 or larger as a function of catalog backazimuth for **a** backazimuth and **b** slowness determined from optimal slowness vector values compared with values from catalog location. Red lines show running means in 30° bins incremented by 5°

spatial aliasing of signals. Another important consideration is the number of array components for which data is available. We require data from at least seven components to analyze an event; otherwise, we deem the array to be too compromised in terms of slowness resolution to be useful. From our assembled dataset, 5124 of the events have data from at least 7 of the 9 array elements, with 14% of the events utilizing all 9 array components and another 69% of the events with data from 8 components.

For each event, we resample the data at 100 samples per second, remove the mean and trend, and bandpass filter between 1 and 4 Hz at each element of the array. We calculate

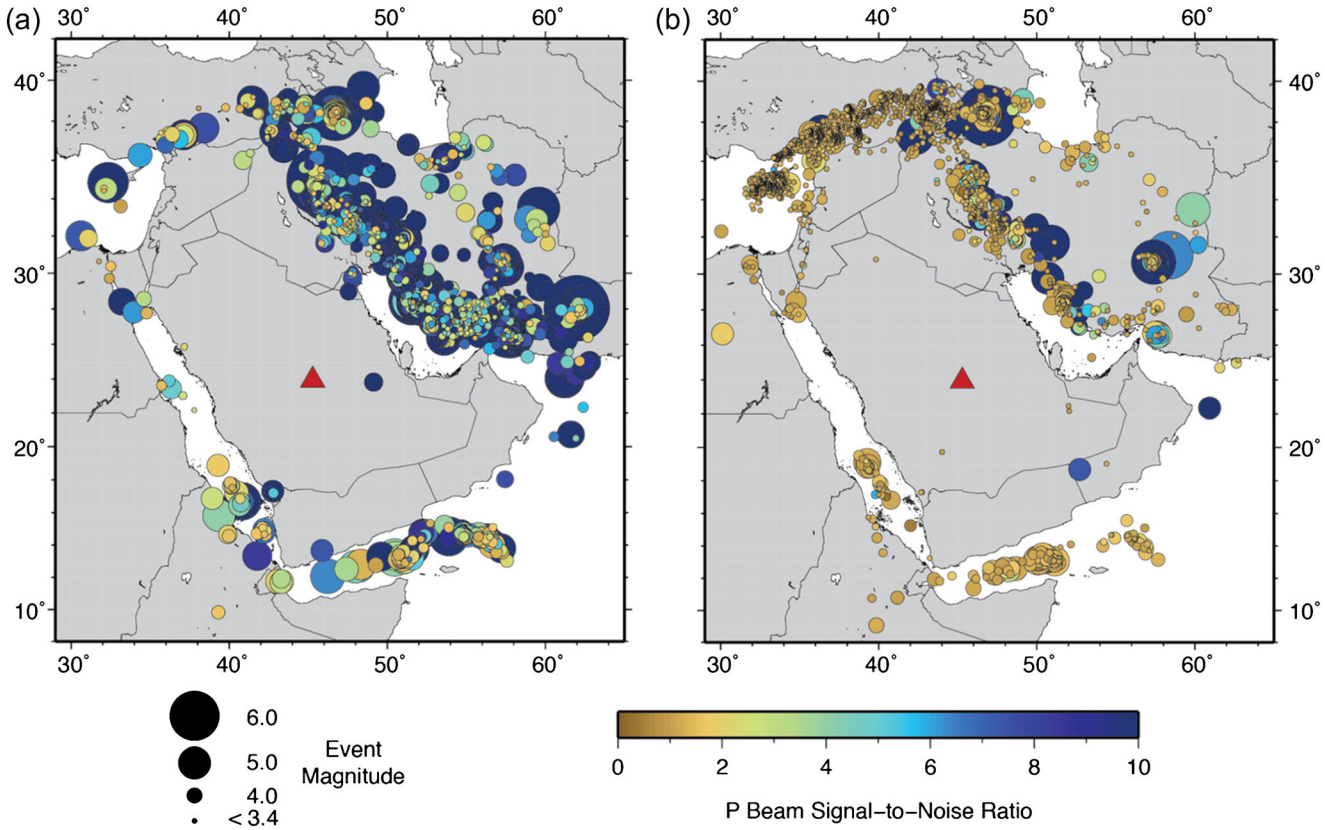

Fig. 4 Map of events that are **a** well detected by the array and **b** not well detected by the array. Color of event indicates the signal-to-noise ratio of the P wave beam compared with the noise-window beam and size of the circle indicates event magnitude

the theoretical arrival time for a particular phase using the event distance and depth from the catalog location and the ak135 travel-time model (Kennett et al. 1995). Windows are cut around the phase using the theoretical arrival time for that phase. We employ a sliding window to account for discrepancies between the theoretical and the actual arrival of the phase due to event mislocation and deviation of the ak135 model from the true velocity structure. The first window begins at 4.0 s before the theoretical arrival time, and we analyze 7 s of data. Subsequent window start times are shifted by 0.5 s, and the final window begins at 6 s after the theoretical arrival time. Each time window is analyzed separately, and the window with the highest power is kept.

We employ a time-domain beam packing scheme (e.g., Schweitzer et al. 2002) to search for the optimal slowness vector in each defined window, similar to a frequency-wavenumber analysis. This method forms beams over a predefined grid of slownesses, and the slowness grid point with the highest power beam determines the optimal slowness vector. Beams are formed using a 4th root process (e.g., Muirhead and Datt 1976), which can help enhance coherent energy and mitigate effects from anomalous traces, and beam power is measured in a root-mean-square sense. An example of the resulting power vs. slowness grid is shown in Fig. 2. We analyze windows for both P and S phases as well as a noise window. The noise window is defined to be 10 s long starting 60 s before the theoretical P wave arrival, and the only difference in analysis is that no sliding window is used.

Array performance

One issue with array analysis is that arrays have been shown to have systematic biases due to lateral heterogeneities that influence the slowness vector determination. Corrections to slowness and backazimuth measurements can be applied to account for these biases providing more accurate phase identification and location estimates (e.g., Bondár et al. 1999). Typically, the calculation of these corrections is made using a set of earthquakes with a high degree of location certainty. The construction of a data set of ground-truth events and formulation of station corrections for the QWAR and HQAR arrays is beyond the scope of this study; however, we do consider the slowness and backazimuth determinations of the QWAR array compared with other IMS arrays. To help limit our observations to instances where the catalog event in question was well-identified by our beampacking analysis, we include in our analysis only events with a P wave signal-to-noise ratio of 2.0. That is, the power of the beam for the P wave window must be at least two times higher than the power of the beam for the noise window. Additionally, to weed out

the worst of the outliers, we also eliminate events for which the backazimuthal residual is greater than 90° or the slowness residual is greater than 10 s/° under the assumption that these measurements do not truly represent the event in question. These simple quality controls exclude many events that are well-located by the array but have weaker signals and cannot completely eliminate instances of high SNRs that are from spurious signals rather than the catalog event. However, the 1558 events that remain should be adequate to provide a reasonable picture of array performance despite the possibility of remaining outliers.

Figure 3 shows slowness and backazimuthal residuals as a function of the catalog backazimuth. Residuals are determined from comparing the P-beam slowness and backazimuth defined by the optimal slowness vector obtained from the beampacking analysis to the theoretical backazimuth and slowness determined from the event's catalog location and the ak135 earth model. For uncorrected IMS arrays, the variance of azimuthal residuals typically falls between 10° and 35°, and the variance of slowness residuals between 1.0 and 2.0 s/° (Bondár et al. 1999). These are measured for teleseismic events, not regional events; however, they provide a baseline for comparison. We bin the residuals we obtain from QWAR in 30° azimuthal bins and calculate a running average for the mean correction to slowness and azimuth with 5° increments for the bins. We find mean azimuthal residuals to be between −28° and 10° with an average residual of approximately 6.8°, and the largest residuals occurring in bins with few events and more numerous likely outliers. The mean slowness residuals range from 0.4 to 3.5 s/°. The average standard deviation is 7.6° for the azimuthal residuals, and 1.5 s/° for the slowness residuals which compares favorably with values of up to approximately 6° and 1.4 s/°, respectively, for IMS arrays. It is also important to consider, as we mention above, that we do not make an attempt to use only events with a high-degree of ground-truth, so we assume that event mislocation contributes significantly to the scatter observed in our results.

Event detection

To better understand the detection capabilities of the QWAR array, we look at which catalog events are well detected by the array compared with those that are not. For these purposes, we define a well-detected event as one in which the slowness and backazimuth determined by the array analysis are within two standard deviations of the mean residual expected for the catalog slowness and backazimuth for that event (Fig. 3), as described above. This definition does not perfectly categorize events but with our large data set should allow us to illuminate some general trends. The events determined to be well-detected are plotted in Fig. 4a, and events that are not well-detected are plotted in Fig. 4b. Of the 5124 events analyzed, 1690 meet the definition of well-detected and fall heavily to the northeast along the Zagros suture zone and the Iranian

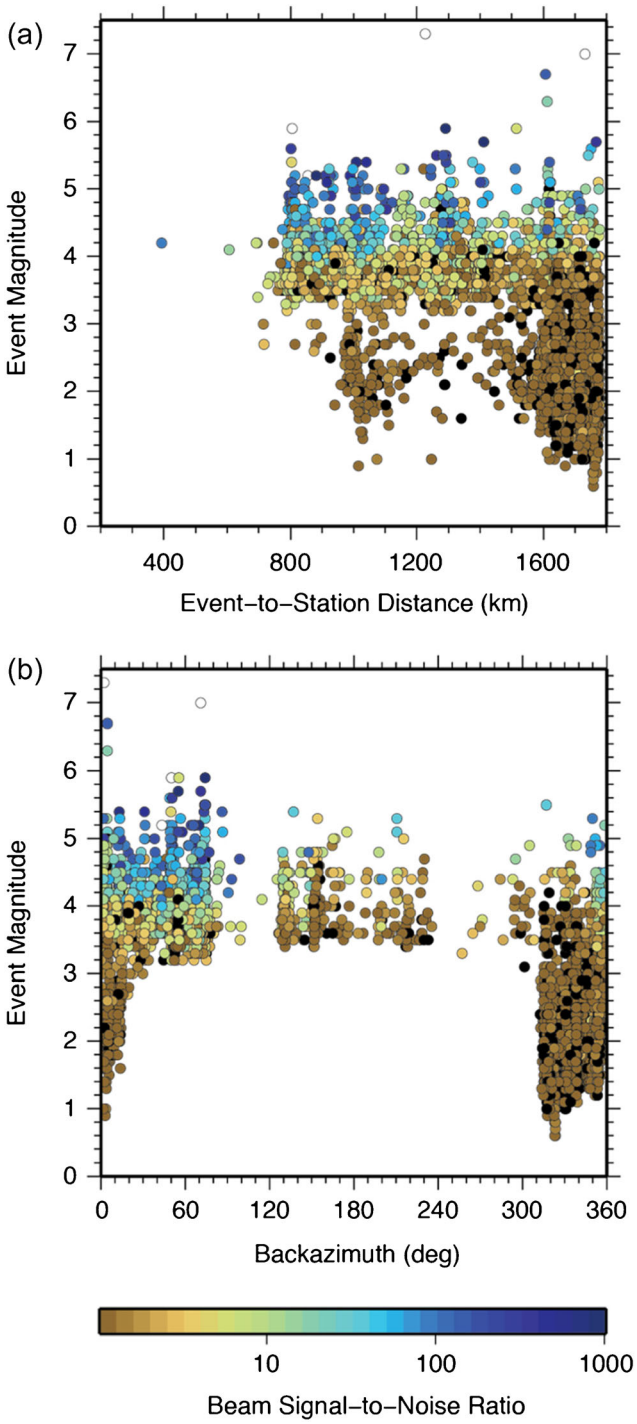

Fig. 5 Beam signal-to-noise ratios as a function of event magnitude and **a** event-to-station distance and **b** backazimuth from the QWAR array. Color of circles indicates the signal-to-noise ratio of the P wave beam compared with the noise-window beam

Plateau. Events along the Bitlis suture to the north and northwest between the Mediterranean Sea and the Caspian Sea are generally poorly detected. A major factor in this trend is due to the combination that the earthquakes in our data set located in this direction extend to smaller magnitudes than in other directions, and they are generally positioned furthest from the

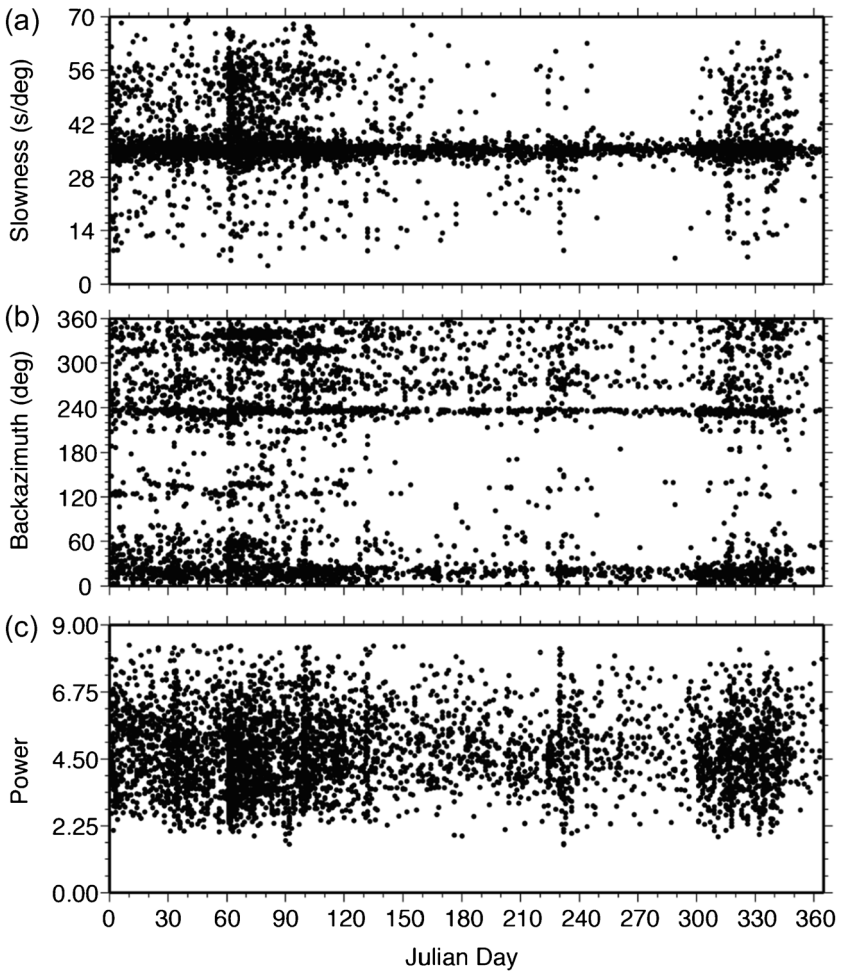

Fig. 6 Optimal slowness vectors from noise windows in terms of **a** slowness, **b** backazimuth, and **c** power, plotted as a function of julian day

array. Figure 5 shows the beam signal-to-noise ratio as functions of event magnitude, distance, and backazimuth to better show how distance and direction affect event detection. Of the 2804 events with magnitudes less than 3.0, 83% of them have backazimuths between approximately 310° and 20°. Less than 2% of these events are detected; however, 88% of these events are at distances greater than 14° from the array. Over 60% of the events with magnitudes between 3 and 4 are detected, and that rises to 82% for events over magnitude 4.0.

One reason for missed detections may be the occurrence of persistent, strong, and nearby noise sources, which in some cases could provide a more coherent signal than small, more distant earthquakes. We further discuss the ambient seismic noise recorded at in the next section. Another factor in event detection is the attenuation of the seismic signals arriving at the array. While attenuation is generally quite low throughout the Arabian Peninsula, several studies have observed very high regional-phase attenuation to the north, northeast, and east along the collision zones of the Zagros suture, the Bitlis suture, and the Turkish and Iranian Plateau (e.g., Pasyanos et al. 2009; Bao et al. 2011; Zhao and Xie 2016). Most of the earthquakes in our dataset travel through these areas of high attenuation. Likely to a lesser extent, other considerations for missed detections include possible event mislocation, and our use of a sliding window, which in some cases may result in more powerful measurement for a window in the coda instead of one encompassing the direct phase. In those cases, if the coda contains local reflections, the slowness vector could be altered from the true direction of the event.

Noise field

We analyze noise windows with every event for which there is data from at least seven array components to better understand the regional noise field and its possible impacts on event detection. An initial observation from the noise-window results is that a number of the optimal slowness vectors had very high power measurements relative to the average power level for all noise windows. We attribute these measurements as likely belonging to earthquakes that are either uncataloged or from events that are spaced closely enough in time that the defined noise window from one event overlaps with the earlier event. To help mitigate the effects of such events on our interpretation of the noise, we discard noise measurements with powers

that are greater than the mean of all the noise measurements. This procedure leaves us with 4776 noise windows and has minimal impact on the overall results. The main consequence is a diminished amount of apparent P wave energy coming from the direction of the Arabian/Persian Gulf that is likely from earthquakes as opposed to true noise sources. In Fig. 6, we plot the optimal slowness vectors of the remaining noise windows in terms of slowness, direction, and power as a function of julian day. A limitation of this plot is that it shows only the location and power of the strongest noise source in each time window and discards information about persistent, but weaker, sources. To compensate for this limitation, we also perform a 2D stacking of all the noise-window slowness grids and plot the results in Fig. 7.

We do not detect any obvious seasonality in noise source location or slowness in contrast to what is often observed (e.g., Koper and de Foy 2008; Zhang et al. 2009; Hillers and Ben-Zion 2011); however, these previous studies focus on high-frequency noise that is generated in the direction of open ocean. In our study, both power and direction show a strong degree of consistency throughout the calendar year that may be due to differing storm and wind patterns in the sheltered water regions surrounding the Arabian Peninsula compared to the ocean. The strongest noise signal in Fig. 7 has a slowness of approximately 35 s/° and a backazimuth of 20°, in the direction of the northern Arabian/Persian Gulf. The second strongest peak has a similar slowness and a backazimuth of 235°, in the direction of the southern Red Sea. Other noise sources also traveling with this slowness appear with weaker power for most of the lengths of the Red Sea and Arabian/Persian Gulf, and also in the direction of the east end of the Mediterranean Sea. A much weaker signal is also seen to the southeast, in the direction of the Arabian Sea. We interpret these noise sources as likely Lg waves generated near the coast of the bodies of water surrounding the Arabian Peninsula. Lg is a crustal phase, composed of multiple post-critical reflection of S-waves, and is often the most prominent phase on a seismogram from regional earthquakes. It typically has a group velocity of 3.0–3.6 km/s; in line with the apparent velocity of 3.2 km/s, we see from our noise window slownesses. Furthermore, Lg noise energy has been observed as a dominant noise source at high frequencies by arrays around the world and appears to be generated primarily in shallow or near-coastal oceanic regions (Koper et al. 2010).

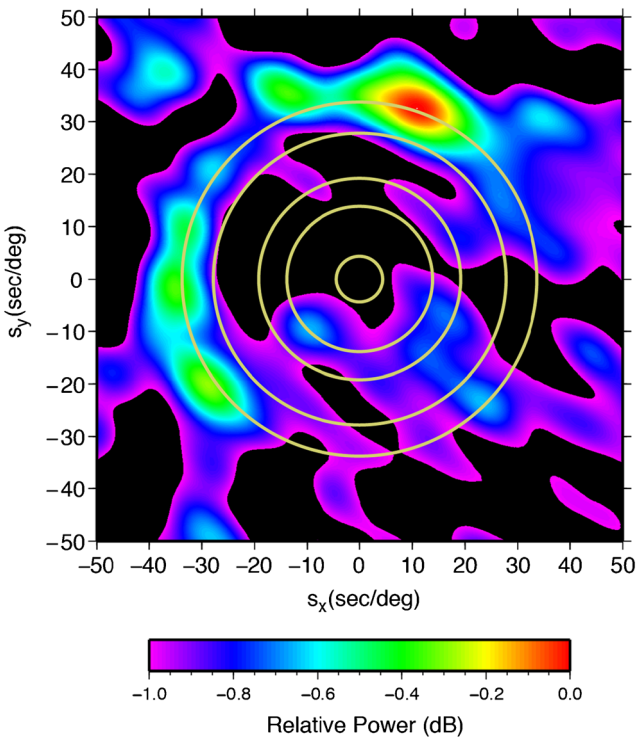

Fig. 7 2D stack of noise-window power vs. slowness grids. Concentric circles show expected slownesses for phases Pdiff, P, Pg, S, and Lg for reference

Although weaker than the Lg noise, a few peaks appear at slownesses corresponding to a Pg phase in the direction of the Arabian Sea. Pg is a crustally traveling regional P wave and has been observed at a few arrays worldwide, but comprises a much smaller portion of the observed global noise composition (Koper et al. 2010). The smaller composition of these wave types may be due to their relatively low power compared with other noise sources, as we see in this study. Additionally, we observe one peak that corresponds to teleseismic P wave velocities to the southwest. Since high-frequency, teleseismic P wave noise has been shown to be most likely generated in the open oceans (e.g., Obrebski et al. 2013; Pyle et al. 2015), this signal may be originating in the South Atlantic Ocean.

Conclusions

We examine the array capabilities of the small-aperture array QWAR in Saudi Arabia. Analysis of the backazimuths and slownesses obtained by a time-domain beampacking method compared with event catalog locations suggest that the array performs well at locating events compared with similar-sized arrays of the IMS. Strong, local, and persistent noise sources in the region as well as high attenuation in the collision zones surrounding the Arabian Peninsula likely play a role in the array's event detection capabilities. A majority of events with magnitudes over 3.0 are detected, rising rapidly to detection rates of over 82% for events with magnitudes over 4.0. The dominant ambient seismic noise sources recorded by the array travel with an apparent velocity consistent with Lg waves. The strongest sources appear to be from the northern Arabian/Persian Gulf and the southern Red Sea, although the Lg energy comes from many directions, and possible weak sources of P wave energy may come from the southeast and southwest.

Acknowledgments We would like to thank Terri Hauk for help with data loading, and two anonymous reviewers for their time and thoughtful comments. This work was performed at Lawrence Livermore National Laboratory under award number DE-AC52-06NA25946. Figures were made using Generic Mapping Tools (GMT) (Wessel and Smith 1991).

References

Al-Hashmi S, Gök R, Al-Toubi K, Al-Shijbi Y, El-Hussain I, Rodgers AJ (2011) Seismic velocity structure at the southeastern margin of the Arabian Peninsula. Geophys J Int 186:782–792. https://doi.org/10.1111/j.1365-246X.2011.05067.x

Bao X, Sandvol E, Zor E, Sakin S, Mohamad R, Gök R, Mellors R, Godoladze T, Yetirmishli G, Türkelli N (2011) Pg attenuation tomography within the northern Middle East. Bull Seismol Soc Am 101(4):1496–1506. https://doi.org/10.1785/0120100316

Bondár I, North RG, Beall G (1999) Teleseismic slowness-azimuth station corrections for the international monitoring system seismic network. Bull Seismol Soc Am 89(4):989–1003

Dewey JF, Hempton MR, Kidd WSF, Saroglu F, Sengör AMC (1986) Shortening of continental lithosphere: the neotectonics of eastern Anatolia – a young collision zone. In: Coward MP, Ries AC (eds) Collision tectonics, Geological Society. London, Special Publications, London, pp 3–36

Hillers G, Ben-Zion Y (2011) Seasonal variations of observed noise amplitudes at 2-18 Hz in Southern California. Geophys J Int 184(2):860–868. https://doi.org/10.1111/j.1365-246X.2010.04886.x

Kennett BL, Engdahl ER, Buland R (1995) Constraints on seismic velocities in the earth from travel times. Geophys J Int 122:108–124

Koper KD, de Foy B (2008) Seasonal anisotropy in short-period seismic noise recorded in South Asia. Bull Seismol Soc Am 98(6):3033–3045. https://doi.org/10.1785/0120080082

Koper KD, Seats K, Benz H (2010) On the composition of Earth's short-period seismic noise field. Bull Seismol Soc Am 100(2):606–617. https://doi.org/10.1785/0120090120

Muirhead KJ, Datt R (1976) The nth root process applied to seismic array data. Geophys J R Astron Soc 47:197–210

Obrebski M, Ardhuin F, Stutzmann E, Schimmel M (2013) Detection of microseismic compressional (P) body waves aided by numerical modeling of oceanic noise sources. J Geophys Res Solid Earth 118:4312–4324. https://doi.org/10.1002/jgrb.50233

Pasyanos ME, Matzel EM, Walter WR, Rodgers AJ (2009) Broad-band Lg attenuation Modelling in the Middle East. Geophys J Int 177:1166–1176. https://doi.org/10.1111/j.1365-246X.2009.04128.x

Pyle ML, Koper KD, Euler GG, Burlacu R (2015) Location of high-frequency P wave microseismic noise in the Pacific Ocean using multiple small aperture arrays. Geophys Res Lett 42:2700–2708. https://doi.org/10.1002/2015GL063530

Schweitzer J, Fyen J, Mykkeltveit S, Kværna T (2002) Chapter 9: seismic arrays. In: Bourmann P (ed) IASPEI new manual of seismological observatory practice. GeoForschungsZentrum, Potsdam, 52 pp

Wessel P, Smith WHF (1991) Free software helps map and display data. EOS Trans AGU 72(441):445–446. https://doi.org/10.1029/90EO00319

Zhang J, Gerstoft P, Shearer PM (2009) High-frequency P-wave seismic noise driven by ocean winds. Geophys Res Lett 36:L09302. https://doi.org/10.1029/2009GL037761

Zhao L-F, Xie X-B (2016) Strong Lg-wave attenuation in the Middle East continental collision Orogenic Belt. Tectonophysics 674:135–146. https://doi.org/10.1016/j.tecto.2016.02.025